JOURNAL OF APPLIED ELECTROCHEMISTRY **26** (1996) 175–185

A model for the Kolbe reaction of acetate in a parallel-plate reactor

J.-F. YAN*, P. S. FEDKIW‡

Department of Chemical Engineering, North Carolina State University, Raleigh, NC 27695-7905, USA

C. G. LAW, Jr.

DuPont Experimental Station, Wilmington, DE 19880-0269, USA

Received 12 December 1994; revised 2 May 1995

A mathematical model is developed for the study of the Kolbe oxidative dimerization of acetate to ethane and carbon dioxide in a parallel-plate reactor operating at a fixed cell potential, with hydrogen evolution being the cathode reaction. The volume of gas evolved into the interelectrode gap is tracked by constructing a hypothetical gas layer which increases in thickness with the streamwise direction in a manner determined by solution to the model equations; concurrently, the liquid flows in a hypothetical layer which decreases in thickness. The three-component gas phase is assumed to be ideal, and the liquid phase is an aqueous mixture of five species: acetate, proton, sodium and hydroxyl ions and acetic acid. The model predicts the concentration profiles and the streamwise variation of the gas–void fraction, reaction current density and liquid and gas velocities. Gas evolution causes a decreasing current density in the streamwise direction and an increasing gas and liquid velocity. The concentrations of acetic acid and proton decrease in the streamwise direction, while hydroxyl concentration increases; the decrease in acetate concentration, however, is not significant until the local base-to-acid ratio is near unity because of the buffering effect from undissociated acetic acid. The average current density increases with inlet solution velocity and cell potential and asymptotically approaches the secondary current limit. There exists an optimal interelectrode separation where the cell resistance is minimum. The average current density exhibits a shallow maximum with the base-to-acid ratio of the feed, but decreases precipitously when the ratio is near unity due to the rapid decrease in the proton concentration.

Nomenclature

b_a	anodic Tafel constant of the Kolbe reaction of acetate (V)
b_c	cathodic Tafel constant of hydrogen evolution reaction (V)
c_1	acetate concentration, mol cm^{-3}
$c_{1,ref}$	reference concentration of acetate (mol cm^{-3})
c_2	acetic acid concentration (mol cm^{-3})
c_3	proton concentration (mol cm^{-3})
$c_{3,ref}$	reference concentration of proton (mol cm^{-3})
c_4	hydroxyl concentration (mol cm^{-3})
c_A	stoichiometric concentration of acetic acid in the feed stream (mol cm^{-3})
c_B	stoichiometric concentration of sodium hydroxide in the feed stream (mol cm^{-3})
$c_{B/A}$	c_B/c_A, base-to-acid ratio in the feed stream (sodium hydroxide to acetic acid)
$c_i(0)$	concentration of species i at cell inlet (mol cm^{-3})
c_i^*	c_i/c_A
E_d	decomposition potential (V)
$E^o_{eq,a}$	standard open-circuit potential of the Kolbe reaction of acetate (V)
$E_{eq,a}$	open-circuit potential of the Kolbe reaction of acetate (V)
$E^o_{eq,c}$	standard open-circuit potential of hydrogen evolution reaction (V)
$E_{eq,c}$	open-circuit potential of hydrogen evolution reaction (V)
F	Faraday constant (96 487 C equiv.$^{-1}$)
f	gas-void fraction
h	cell height (cm)
IR	ohmic-voltage drop in the electrolyte (V)
i	current density (A cm^{-2})
$i_{a,ref}$	exchange current density of acetate Kolbe reaction at reference concentration (A cm^{-2})
$i_{c,ref}$	exchange current density of hydrogen evolution reaction at a reference concentration (A cm^{-2})
i_{avg}	average current density (A cm^{-2})
$i(0)$	current density at the inlet of the cell (A cm^{-2})
i^*	$i/i(0)$
K_a	ionization constant of acetic acid (mol cm^{-3})
K_a^*	K_a/c_A

* Present address: Philips Components, 6701 St. Andrews, Columbia, SC, 29212, USA.
‡ Author to whom to address correspondence.

0021-891X

K_w ionization constant of water ($mol^2\,cm^{-6}$)
K_w^* K_w/c_A^2
P pressure (atm)
p_5 partial pressure of ethane (atm)
p_6 partial pressure of carbon dioxide (atm)
p_7 partial pressure of hydrogen (atm)
q_a reaction order of acetate in Kolbe reaction
q_c reaction order of proton in hydrogen evolution reaction
R gas constant ($82.05\,atm\,cm^3\,mol^{-1}\,K^{-1}$)
T temperature (K)
V_T cell potential (V)
V_T^* V_TF/RT
V_a anode potential (V)
V_c cathode potential (V)
v_G gas velocity ($cm\,s^{-1}$)
v_G^* v_G/v_0
v_L liquid velocity ($cm\,s^{-1}$)
v_L^* v_L/v_0
v_0 solution velocity at the inlet of the cell ($cm\,s^{-1}$)
w electrode width (cm)
x streamwise coordinate (cm)
x^* x/h

Greek characters

α velocity slip ratio
δ interelectrode separation (cm)
δ_G thickness of gas phase (cm)
δ_L thickness of liquid phase (cm)
η_a anodic overpotential (V)
η_c cathodic overpotential (V)
ρ resistivity of bubble-filled solution (Ω cm)
ρ_0 resistivity of bubble-free solution (Ω cm)

1. Introduction

The Kolbe reaction is the anodic oxidation of a carboxylate moiety in an organic acid with subsequent decarboxylation and coupling to yield a dimer of the alkyl function in the carboxylate reactant [1]. The first and perhaps best known example of the Kolbe reaction is the electrolysis of acetate

$$2CH_3COO^- \longrightarrow CH_3CH_3 + 2CO_2 + 2e^- \quad (1)$$

where carbon dioxide and ethane evolve as gases from the anode. The corresponding cathode reaction is usually proton reduction

$$2H^+ + 2e^- \longrightarrow H_2 \quad (2)$$

with hydrogen gas evolution from the electrode. The anodic and cathodic-product gases disperse as bubbles in the electrolyte and form a gas–liquid mixture which causes an increased ionic resistance and a higher mass-transfer coefficient at the electrode–solution interface [2, 3].

This report presents a reaction-engineering model for the Kolbe oxidation of acetate in a parallel-plate reactor operating at a fixed cell potential. Despite the historical significance of this reaction, to our knowledge a first-principles based model of a Kolbe reaction in a parallel-plate reactor, useful for design, scaleup and parametric studies, has not been presented in the literature; however, Beck has presented an analysis for a radial capillary-gap cell [4]. In consideration that Kolbe electrolysis is an integral step in the production of sebasic acid in which a parallel-plate electrolyser is used [5, 6], it is advantageous to fill this void. The present model is a contribution to this effort and accounts for gas evolution and its effects upon the local reaction current density. The model also considers the homogeneous acid-base reactions to be at equilibrium in the bulk solution. The main limitation of the present model is the neglect of mass-transfer resistance from the bulk solution to the electrode surface. But, because of the buffering effect of undissociated acetic acid in the diffusion layer, mass-transfer resistance is expected to be an important concern only when the solution velocity is low. Another limitation of the model is the assumed constant bubble-free resistivity. In reality, the bubble-free resistivity is a function of solution concentration of the electrolytes which will vary in the streamwise direction due to material consumption by the electrochemical reactions. Nevertheless, the present formulation is useful in understanding and quantifying the complex chemical and physical processes occurring in a Kolbe reactor and serves as a basis for a more complete treatment.

2. Model development

The electrochemical cell under consideration is shown in Fig. 1 and is a parallel-plate reactor with height h, width w, and interelectrode separation δ, with no separator between the two. Gas is generated at both electrodes and disperses into the electrolyte, as shown in Fig. 2(a). As a major simplification of the complex, two-phase flow, we assume that the evolved gaseous products define a hypothetical gas layer of thickness δ_G which increases with streamwise direction, as shown in Fig. 2(b). The liquid is, consequently, confined to a layer of thickness $\delta - \delta_G$. We further assume that the gas and liquid are well-mixed and flow at a plug-flow velocity v_G and v_L, respectively, and mass transport is by convection only. The gas does not completely block ionic flow, as might be inferred from Fig. 2(b), but rather defines an equivalent gas-layer thickness if all bubbles were to coalesce at any particular streamwise position. The presence of the gas does, however, increase the local ionic resistance which is taken into account in the model. Our approach is similar to that used by Funk and Thorpe [7] who modelled a parallel-plate water electrolyser in which oxygen and hydrogen evolve from the anode and the cathode, respectively.

The feed to the reactor is an aqueous mixture of acetic acid and sodium hydroxide of stoichiometric

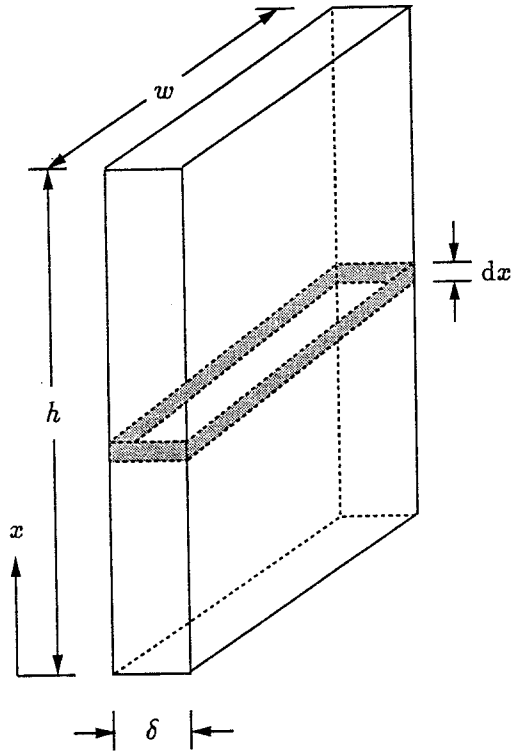

Fig. 1. Schematic of a parallel-plate reactor.

concentration c_A and c_B, respectively, with the base being used to increase the solution conductivity. The liquid is assumed to be saturated with ethane, carbon dioxide, and hydrogen. In the development presented below, seven species are numbered in the following way for notational convenience: (1), acetate (CH_3COO^-); (2), acetic acid (CH_3COOH); (3), proton (H^+), (4), hydroxyl (OH^-); (5), ethane (CH_3CH_3); (6), carbon dioxide (CO_2); and (7), hydrogen (H_2). Sodium ion does not need to be considered since it is not involved in any reactions and its concentration remains constant at c_B.

Acetic acid dissociates as

$$CH_3COOH \rightleftharpoons CH_3COO^- + H^+ \qquad (3)$$

with the three concentrations at equilibrium related by

$$K_a = \frac{c_1 c_3}{c_2} \qquad (4)$$

where K_a is the ionization constant of the acid. A second important homogeneous reaction is water ionization

$$H_2O \rightleftharpoons H^+ + OH^- \qquad (5)$$

with proton and hydroxyl concentrations at equilibrium related by

$$K_w = c_3 c_4 \qquad (6)$$

where K_w is the ionization constant of water. We

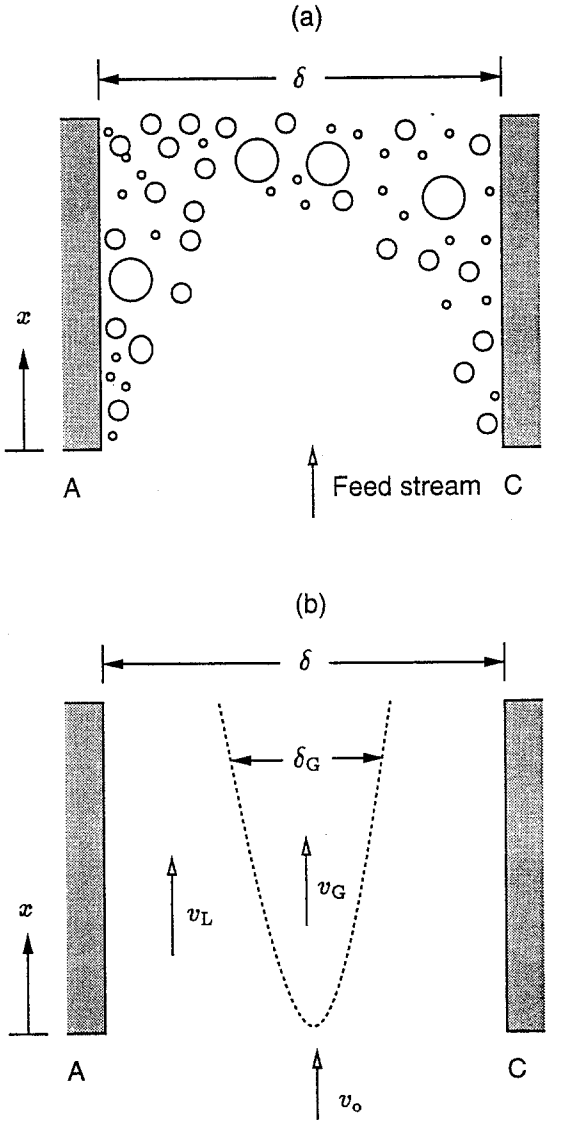

Fig. 2. (a) Cross-section view of a bubble-filled parallel-plate reactor; (b) equivalent gas layer used in the parallel-plate reactor model.

assume that the two acid-base reactions are in equilibrium. We further assume that there is no electronic ohmic-voltage drop and the flow of ionic current is unidirectional and perpendicular to the streamwise direction. Also, as a consequence of the assumed applicability of the ideal gas law, the partial pressure of each component is constant throughout the reactor and proportional to the assumed constant total pressure P according to the stoichiometry in Reactions 1 and 2; that is, $p_5 = P/4$, $p_6 = P/2$, and $p_7 = P/4$, where p_5, p_6, and p_7 represent the partial pressure of ethane, carbon dioxide, and hydrogen, respectively. Finally, we assume that the Kolbe reaction is the only anode reaction and hydrogen evolution is the single cathode reaction.

On the basis of the assumptions presented above, a one-dimensional model is developed in which quantities (concentrations of acetate, acetic acid, proton, and hydroxyl, liquid and gas velocities, local current density, and local gas-void fraction) vary only in the streamwise direction. Under steady-state conditions, the local mole-balance equations for acetate and

acetic acid, respectively, are

$$\frac{\mathrm{d}[(\delta-\delta_G)c_1 v_L]}{\mathrm{d}x} = \frac{-i}{F} + (\delta-\delta_G)R_{HA} \quad (7)$$

$$\frac{\mathrm{d}[(\delta-\delta_G)c_2 v_L]}{\mathrm{d}x} = -(\delta-\delta_G)R_{HA} \quad (8)$$

where i is the local reaction current density and R_{HA} represents the dissociation rate of acetic acid. Addition of Equations 7 and 8 results in

$$\frac{\mathrm{d}[(\delta-\delta_G)(c_1+c_2)v_L]}{\mathrm{d}x} = \frac{-i}{F} \quad (9)$$

which is a balance for total acetate (acetic acid and acetate) and is advantageous to use since it does not contain the homogeneous reaction term. Moreover, since the solution is electroneutral, the charged species obey the charge-conservation principle

$$c_1 + c_4 = c_3 + c_B \quad (10)$$

In summary, Equations 4, 6, 9 and 10 are the governing equations for the four species (acetate, acetic acid, proton and hydroxyl) that must be considered in the liquid layer.

The reaction rate at the anode is expressed by a Tafel-like equation

$$i = i_{a,ref}\left(\frac{c_1}{c_{1,ref}}\right)^{q_a}\exp\left(\frac{V_a - E_{eq,a}}{b_a}\right) \quad (11)$$

where $i_{a,ref}$ is the exchange current density of the Kolbe reaction of acetate at a reference acetate concentration $c_{1,ref}$, q_a is the reaction order of acetate, V_a is the anode potential, and b_a is the anodic Tafel constant. The open-circuit potential $E_{eq,a}$ of the Kolbe reaction is determined from the Nernst equation as

$$E_{eq,a} = E^\circ_{eq,a} + \frac{RT}{2F}\ln\left(\frac{p_5 p_6^2}{c_1^2}\right) \quad (12)$$

where $E^\circ_{eq,a}$ is the standard open-circuit potential. Similarly, the hydrogen evolution reaction kinetics at the cathode may be expressed as

$$i = i_{c,ref}\left(\frac{c_3}{c_{3,ref}}\right)^{q_c}\exp\left(-\frac{(Vc - E_{eq,c})}{b_c}\right) \quad (13)$$

where $i_{c,ref}$ is the exchange current density of the hydrogen reaction at a reference proton concentration $c_{3,ref}$, q_c is the reaction order of proton, V_c is the cathode potential, and b_c is the cathodic Tafel constant. The open-circuit potential $E_{eq,c}$ of the hydrogen evolution reaction is determined from the Nernst equation as

$$E_{eq,c} = E^\circ_{eq,c} + \frac{RT}{2F}\ln\left(\frac{c_3^2}{p_7}\right) \quad (14)$$

where $E^\circ_{eq,c}$ is the standard open-circuit potential. Equation 11 is essentially that proposed by Vassiliev *et al.* [8] for the Kolbe reaction of acetate, and Equation 13 is the reaction kinetics for irreversible hydrogen evolution and has been widely used by others (e.g. [9, 10]).

The cell voltage V_T can be considered as the sum of four contributions: the thermodynamic decomposition potential E_d, the anode overpotential η_a, the cathode overpotential $-\eta_c$, and the ohmic-voltage drop IR; that is,

$$\begin{aligned} V_T &= E_d + \eta_a - \eta_c + IR \\ &= \left\{(E^\circ_a - E^\circ_c) + \frac{RT}{2F}\ln\left[\frac{p_5 p_6^2 p_7}{(c_1 c_3)^2}\right]\right\} + \\ &\quad \left\{b_a \ln\left[\frac{i}{i_{a,ref}(c_1/c_{1,ref})^{q_a}}\right]\right\} + \\ &\quad \left\{b_c \ln\left[\frac{i}{i_{c,ref}(c_3/c_{3,ref})^{q_c}}\right]\right\} + \\ &\quad \left\{i\rho_0\delta\left(1-\frac{\delta_G}{\delta}\right)^{-1.5}\right\} \end{aligned} \quad (15)$$

In Equation 15, the Bruggeman equation [11] has been used in the last term in braces to relate the resistivity ρ of the bubble-filled solution to that of the bubble-free solution ρ_0

$$\rho = \rho_0(1-f)^{-1.5} \quad (16)$$

where the local gas-void fraction f is equal to δ_G/δ according to Fig. 2(b).

The liquid and gas velocities are obtained by dividing the appropriate volumetric flow rate by the cross-sectional area of the liquid or gas layer. Thus, the gas velocity v_G is calculated from

$$\delta_G v_G = \frac{2RT}{FP}\int_0^x i\mathrm{d}x \quad (17)$$

And, assuming that the liquid volumetric flow rate is constant, the liquid velocity v_L is evaluated from

$$(\delta-\delta_G)v_L = v_0\delta \quad (18)$$

Table 1. Dimensionless groups

Symbol	*Definition*
β_a	$\frac{b_a F}{RT}$
β_c	$\frac{b_c F}{RT}$
K_1	$\frac{i(0)h}{c_A v_0 \delta F}$
K_2	$\frac{F}{RT}\left\{(E^\circ_a - E^\circ_c) + \frac{RT}{2F}\ln\left[\frac{p_5 p_6^2 p_7}{(c_A)^4}\right]\right\} + \beta_a \ln\left[\frac{i(0)}{i_{a,ref}(c_A/c_{1,ref})^{q_a}}\right] + \beta_c \ln\left[\frac{i(0)}{i_{c,ref}(c_A/c_{3,ref})^{q_c}}\right]$
K_3	$\frac{F}{RT} i(0)\rho_0\delta$
K_4	$\frac{i(0)h}{v_0\delta F}\frac{2RT}{P}$

Furthermore, the slip ratio α, defined as the gas velocity divided by the liquid velocity,

$$\alpha = \frac{v_G}{v_L} \tag{19}$$

is set *a priori* in our model and is applied for $x > 0$. The slip ratio for oxygen and hydrogen in water electrolysis was determined experimentally by Funk and Thorpe [7] as near unity.

By defining dimensionless variables, the governing equations (Equations 4, 6, 9, 10, 15, 17–19) become

$$\frac{d}{dx^*}[(1-f)(c_1^* + c_2^*)v_L^*] = -K_1 i^* \tag{20}$$

$$K_a^* = \frac{c_1^* c_3^*}{c_2^*} \tag{21}$$

$$K_w^* = c_3^* c_4^* \tag{22}$$

$$c_1^* + c_4^* = c_3^* + c_{B/A} \tag{23}$$

$$V_T^* = K_2 - \ln[(c_1^*)^{1+q_a\beta_a}(c_3^*)^{1+q_c\beta_c}] + (\beta_a + \beta_c)\ln i^* + K_3(1-f)^{-1.5} i^* \tag{24}$$

$$fv_G^* = K_4 \int_0^{x^*} i^* dx^* \tag{25}$$

$$v_L^* = (1-f)^{-1} \tag{26}$$

$$\alpha = \frac{v_G^*}{v_L^*} \tag{27}$$

Dimensionless variables are defined in the Nomenclature; dimensionless groups are listed in Table 1.

To reduce the numerical burden, mathematical manipulations were carried out to halve the number of unknowns from the eight explicit in Equations 20–27: $c_k^*(k = 1\text{–}4)$, v_L^*, v_G^*, i^* and f. First, Equations 20–23 and Equation 26 can be manipulated to derive differential equations for c_1^* and c_3^* as

$$\frac{dc_1^*}{dx^*} = \frac{-K_1 i^*}{1 + B(c_1^*)} \tag{28}$$

and

$$\frac{dc_3^*}{dx^*} = \frac{K_1 i^*[c_3^* - K_a^* B(c_1^*)]}{[1 + B(c_1^*)]c_1^*} \tag{29}$$

where the positive quantity $B(c_1^*)$ is defined by

$$B(c_1^*) = \frac{1}{2K_a^*}\left\{2c_i^* - c_{B/A} - \frac{(c_{B/A} - c_1^*)c_1^*}{[(c_{B/A} - c_1^*)^2 + 4K_w^*]^{1/2}} + [(c_{B/A} - c_1^*)^2 + 4K_w^*]^{1/2}\right\} \tag{30}$$

Second, by taking the derivative of fv_G^* with respect to x^*, Equation 25 becomes

$$\frac{d(fv_G^*)}{dx^*} = K_4 i^* \tag{31}$$

and combination of equations 26, 27 and 31 yields the governing equation for f as

$$\frac{df}{dx^*} = \frac{K_4 i^*(1-f)^2}{\alpha} \tag{32}$$

Finally, by taking the derivative of V_T^* with respect to x^* and recognizing this quantity is zero, Equation 24 can be rearranged to yield the governing equation for i^* as

$$\frac{di^*}{dx^*} = \frac{[(1+q_c\beta_c)(c_3^*)^{-1}\frac{dc_3^*}{dx^*} + (1+q_a\beta_a)(c_1^*)^{-1}\frac{dc_1^*}{dx^*} - 1.5K_3 i^*(1-f)^{-2.5}\frac{df}{dx^*}]}{(\beta_a + \beta_c)/i^* + K_3(1-f)^{-1.5}} \tag{33}$$

Equations 28, 29, 32 and 33 constitute the governing equations for c_1^*, c_3^*, f and i^*, respectively.

The concentrations of acetate and proton, the gas-layer thickness, and the current density are the specified inlet conditions at $x = 0$ and are given as

$$c_i = c_i(0) \qquad i = 1, 3 \tag{34}$$

$$\delta_G = 0 \tag{35}$$

$$i = i(0) \tag{36}$$

The current density at the inlet of the reactor $i(0)$ actually is not known *a priori*, but it is obtained by solving numerically Equation 15 at $x = 0$ since all terms except i are known. Also, the inlet concentrations of acetate, acetic acid, proton and hydroxyl, are determined by simultaneously solving Equations 4, 6, 10 and a total acetate balance at the reactor inlet

$$c_A = c_1 + c_2 \tag{37}$$

In a dimensionless format, the inlet conditions become

$$c_i^* = c_i^*(0) \qquad i = 1, 3 \tag{38}$$

$$f = 0 \tag{39}$$

$$i^* = 1 \tag{40}$$

3. Method of solution

The equilibrium liquid concentrations in the inlet stream to the reactor were found by numerically solving a nondimensional form of Equations 4, 6, 10 and 37 using the subroutine DNEQNF of IMSL [12]. The inlet current density was found by solving Equation 24 numerically also using the subroutine DNEQNF.

Equations 28, 29, 32 and 33 were numerically integrated using the Gear method IMSL subroutine DIVPAG [12] to give c_1^*, c_3^*, f and i^* at different x^* from which c_2^* and c_4^* are calculated by Equations 21 and 22, and v_L^* and v_G^* are calculated by Equations 26 and 27, respectively.

As a means to test the numerical consistency of the model, the average current density at five different

Table 2. Parameters used in the calculations

δ	= 1 cm
h	= 100 cm
V_T	= 5.0 V
P	= 1 atm
T	= 298.15 K
v_0	= 20 cm s^{-1}
ρ_0	= 2.5 Ω cm
α	= 1.0
K_a	= 1.8 × 10^{-8} mol cm^{-3} ([15])
K_w	= 1.0 × 10^{-20} mol^2 cm^{-6} ([15])
c_A	= 1.0 × 10^{-4} mol cm^{-3}
$c_{B/A}$	= 0.5
$c_{1,ref}$	= 1.0 × 10^{-3} mol cm^{-3} ([14])
$c_{3,ref}$	= 1.8 × 10^{-8} mol cm^{-3} ([13])
E_a^o	= 0.396 V ([1])
E_c^o	= 0.0 V ([13])
b_a	= 0.072 V ([14])
b_c	= 0.048 V ([13])
q_a	= 1.0
q_c	= 1.0
$i_{a,ref}$	= 1.9 × 10^{-18} A cm^{-2} (Calculated from Fig. 1 in [14])
$i_{c,ref}$	= 6.8 × 10^{-5} A cm^{-2} ([13])

values of the base-to-acid ratio (0, 0.1, 0.5, 0.9 and 1.0) was calculated by three methods: the mole balance of total acetate, the mole balance of ethane, and the integration of the local current density. The results showed good agreement among the three with a maximum deviation of less than 0.1% which occurred for a base-to-acid ratio of unity.

4. Results and discussion

The parameters used in the calculations are listed in Table 2. The thermodynamic and kinetic constants were obtained from the literature, except for α, q_a, and q_c for lack of published data; consequently, arbitrary, but feasible, values were assigned to the reaction-order parameters q_a and q_c. The slip ratio α was set equal to unity based upon Funk and Thorpe's work with hydrogen and oxygen mixtures in water, and the parameters for cell geometry and operating conditions were chosen to be in a reasonable range.

4.1. *Equilibrium concentrations and current density at reactor inlet*

Figure 3 shows the equilibrium concentration of acetate, acetic acid, proton, and hydroxyl in the feed solution as a function of the base-to-acid ratio. The addition of sodium hydroxide increases the degree of ionization of acetic acid and, hence, the acetate concentration. Clearly the base-to-acid ratio is critical in setting the concentrations of species in the liquid phase, especially at values near unity where there is a large change in the solution pH.

The reaction current density at the reactor inlet $i(0)$ as a function of cell potential is shown in Fig. 4 at three values of the base-to-acid ratio. Since, by assumption, the electrochemical reactions are not mass-transfer limited, the reaction current density continuously increases with cell potential. The straight lines in Fig. 4 indicate that ohmic-voltage drop dominates when the cell potential is greater than 6 V for all base-to-acid ratios. And at any given cell voltage, there are two opposing effects of an increasing base-to-acid ratio: The exchange current density for the Kolbe reaction increases with the base-to-acid ratio because of the increasing acetate concentration, but the exchange current density for hydrogen evolution decreases because of the decreasing proton concentration. The net influence depends on the acetate and proton concentrations and the particular values of the kinetic parameters and, for the conditions used here, leads to a maximum current density with varying $c_{B/A}$.

4.2. *Concentration, gas-void fraction, current density, and velocity profiles*

Figure 5 shows the concentration profiles of acetate, acetic acid, proton, and hydroxyl at a cell voltage

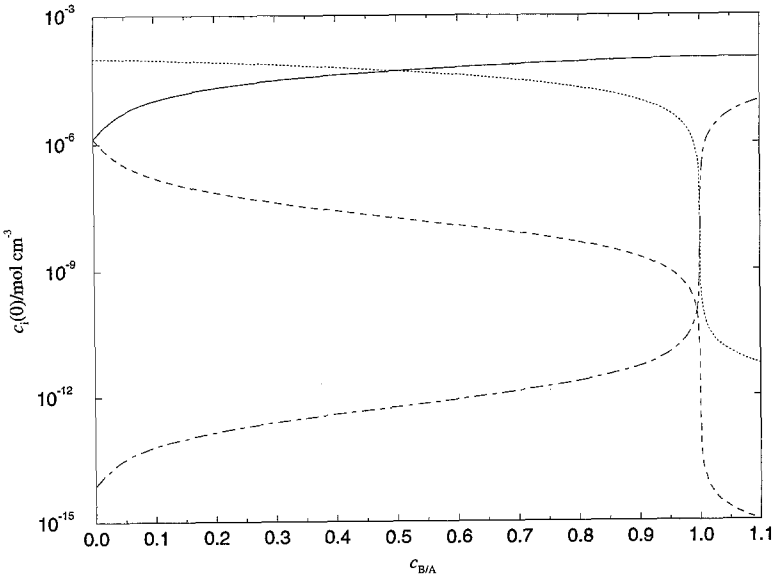

Fig. 3. Equilibrium inlet concentrations as a function of the base-to-acid ratio of the feed. Key: (——) acetate, (·····) acetic acid, (· –) proton and (– - –) hydroxyl.

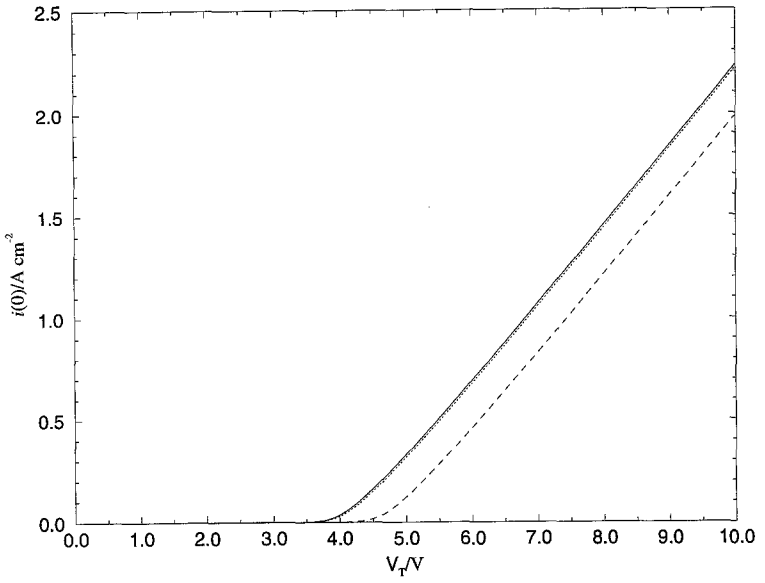

Fig. 4. Current density at reactor inlet as a function of cell potential at three base-to-acid ratios of the feed. Key: (·····) $c_{B/A} = 0$; (——) $c_{B/A} = 0.5$; (– – –) $c_{B/A} = 1.0$.

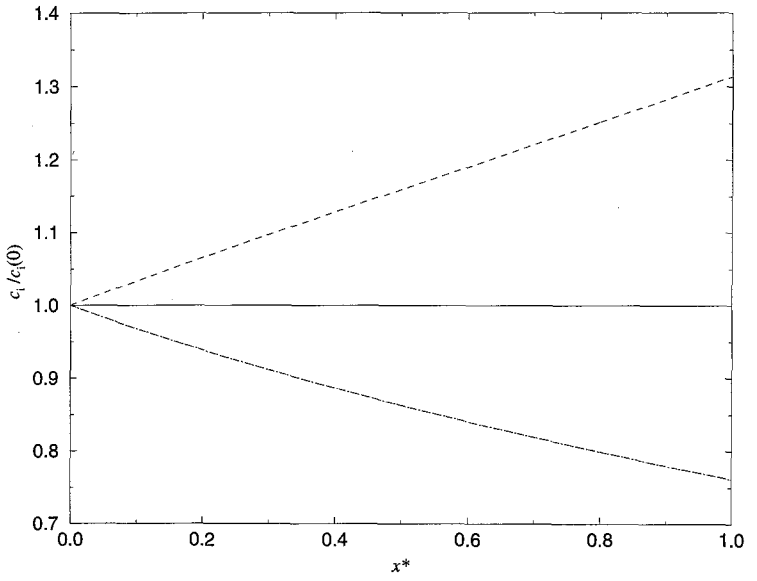

Fig. 5. Streamwise variation of liquid–phase concentrations. Key: (— — —) hydroxyl; (——) acetate; (· – · –) acetic acid and proton.

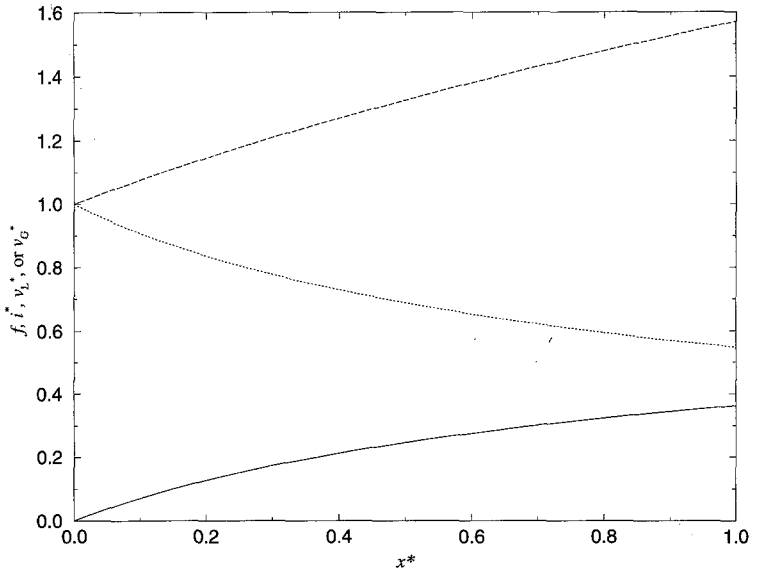

Fig. 6. Streamwise variation of gas–void fraction, current density, and liquid and gas velocities. Key: (——) f; (·····) i^*; (– – –) $v_L^* = v_G^*$.

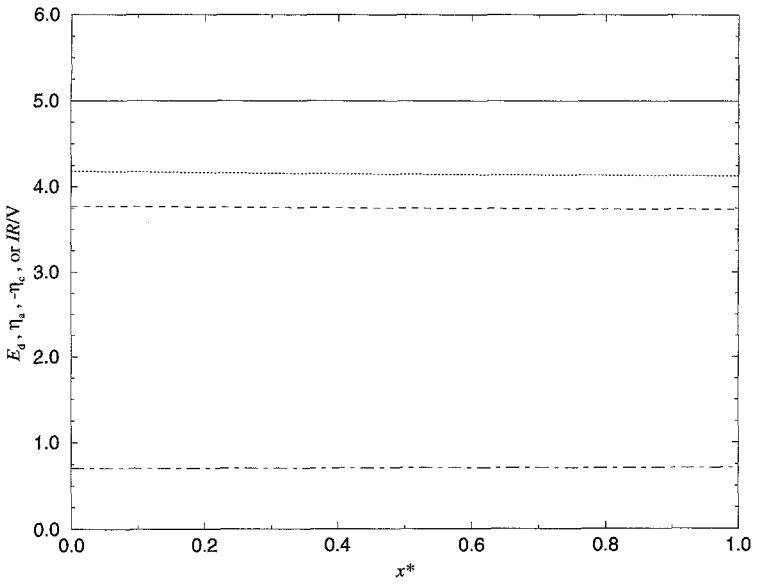

Fig. 7. Streamwise variation of voltage losses contributing to a 5 V cell potential ($v_0 = 20\,\mathrm{cm\,s^{-1}}$). Key: (– · – ·) E_d; (— — —) $E_d + \eta_a$; (·····) $E_d + \eta_a - \eta_c$; (——) $E_d + \eta_a - \eta_c + IR = V_T$.

of 5 V and a base-to-acid ratio in the feed of 0.5. Although acetate is consumed at the anode, there is no significant decrease in its concentration because of the buffering effect by acetic acid, the concentration of which does decrease. Figure 5 also indicates that the solution becomes more basic in the streamwise direction which results from two effects: (i) the consumption of proton in the cathode reaction, and (ii) the decrease in proton concentration in equilibrium with the decreased acetic acid content. Figure 6 shows the corresponding variation of gas–void fraction, current density, and liquid and gas velocities in the streamwise direction. The gas-void fraction increases along the reactor from 0 to 0.38 as a result of the gas evolution. Because of the consequential increase in ionic resistance, the local current density decreases. The gas velocity increases due to the increasing gas volumetric flow rate, and the liquid velocity commensurately increases because of the smaller cross-section area for liquid flow.

4.3. *Cell potential balance*

Figure 7 shows the streamwise variation of the thermodynamic decomposition potential E_d, the anodic overpotential η_a, the cathodic overpotential $-\eta_c$, and the ohmic-voltage drop IR, which all sum to the cell potential of 5 V at any given position. These results correspond to the same reactor conditions used to construct Figs 5 and 6. Because of the low exchange current density for the Kolbe oxidation of acetate, the anode overpotential is the dominant voltage loss. The decomposition potential slightly increases because of the decrease in acetate and proton concentrations. The ohmic-voltage drop also increases slightly because of the increasing gas–void fraction which results in a higher solution resistivity. The increase in ohmic-voltage drop, however, is not as large as one might expect from the increasing gas-void fraction because of the concurrent decrease in the local current density under cell-potential control.

As a means to illustrate a case in which a rapid

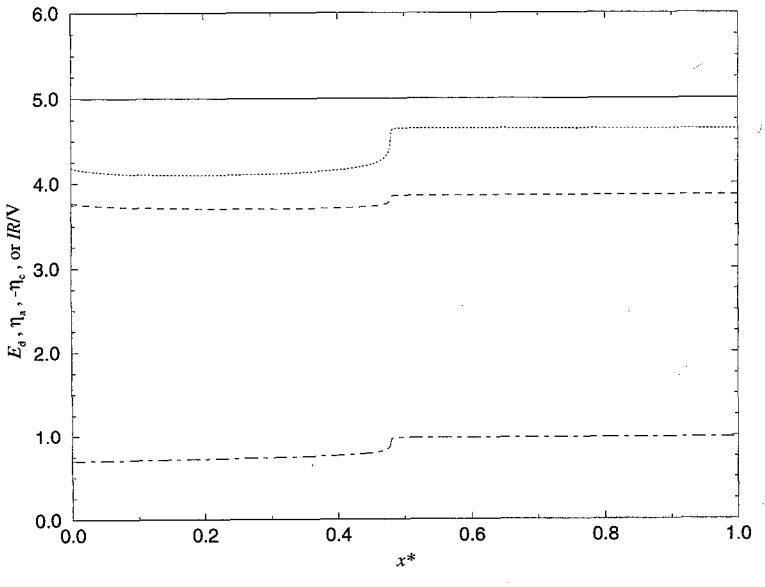

Fig. 8. Streamwise variation of voltage losses contributing to a 5 V cell potential ($v_0 = 1\,\mathrm{cm\,s^{-1}}$). Key: (– – – –) E_d; (— — —) $E_d + \eta_a$; (·····) $E_d + \eta_a - \eta_c$; (——) $E_d + \eta_a - \eta_c + IR = V_T$.

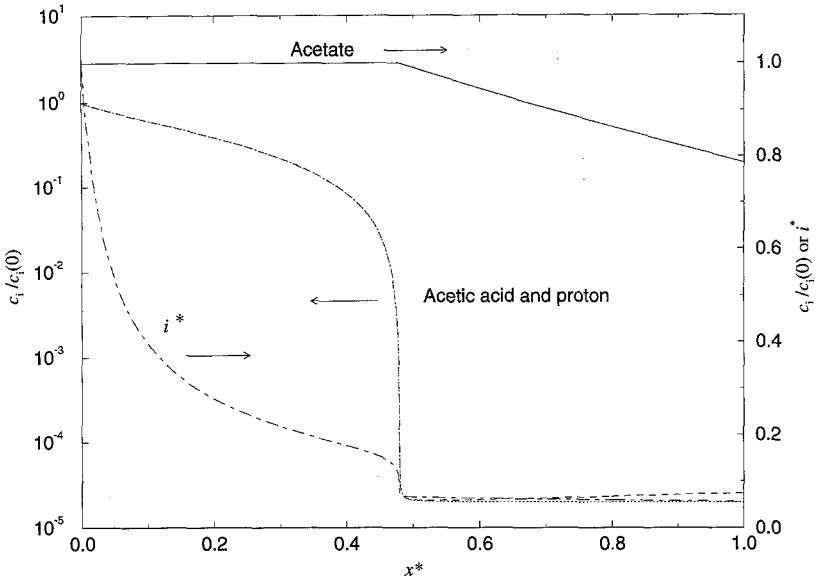

Fig. 9. Streamwise variation of liquid-phase concentrations and current density ($v_0 = 1$ cm s^{-1}).

change in the various elements contributing to a 5 V cell potential occurs, Fig. 8 shows the streamwise variations when the inlet velocity is lowered by a factor of 20 to 1 cm s^{-1} with all other conditions remaining unchanged from those used to construct Fig. 7. At this velocity, the total acetate conversion is higher (~0.61) and, as shown in Fig. 9, a rapid change in the acetate, acetic acid, and proton concentration profiles occurs near $x^* = 0.48$ due to the local base-to-acid ratio approaching unit. A resultant effect is the sudden decrease in the reaction current density, also plotted on the same figure.

4.4. *Parametric studies*

We have used the model to investigate the effects on the average current density of the (i) inlet solution velocity, (ii) interelectrode separation, (iii) base-to-acid ratio of the feed, and (iv) cell potential. These results are shown in Figs 10–13 and discussed below. The cell potential is 5 V and the base-to-acid ratio is 0.5 and all other parameters are equal to those given in Table 2 unless otherwise specified.

With increasing inlet solution velocity, gas is removed more quickly from the cell which results in a lower gas–void fraction. Thus, the average current density increases with the inlet solution velocity as shown in Fig. 10. The increase is most rapid when the inlet solution velocity is near zero, at which the total acetate conversion is high. At high inlet solution velocity, the average current density approaches an asymptotic limit which is equal to the reaction current density at the reactor inlet, as indicated in the figure. Simultaneously, the average gas–void fraction and total acetate conversion both approach zero.

The effect of the interelectrode separation δ on various streamwise-average quantities is shown in Fig. 11. The average current density passes through a maximum which occurs at an optimum interelectrode separation of about 0.35 cm for the parameter set chosen for this calculation. When the separation is lower than 0.35 cm, the average current density drops with decreasing δ because the increasing gas–void fraction affects a larger solution resistance; when the interelectrode separation is larger than

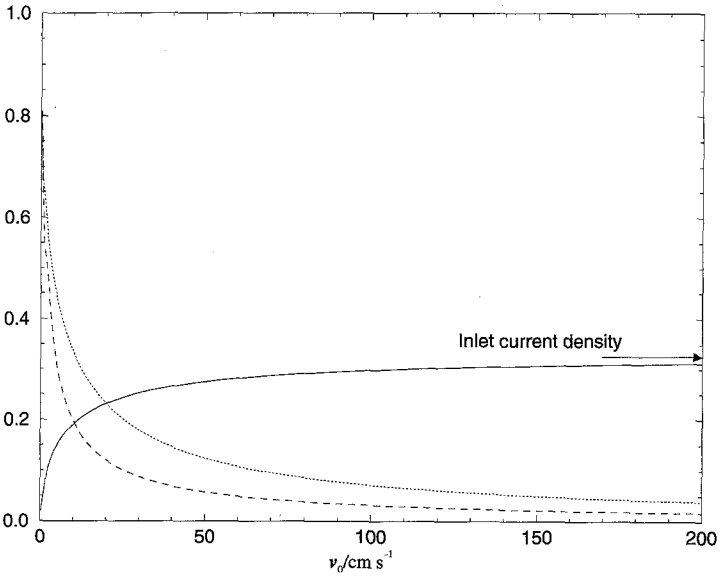

Fig. 10. Effect of varying inlet solution velocity. Key: (——) i_{avg}/A cm^{-2}; (·····) f_{avg}; (– – –) total acetate conversion.

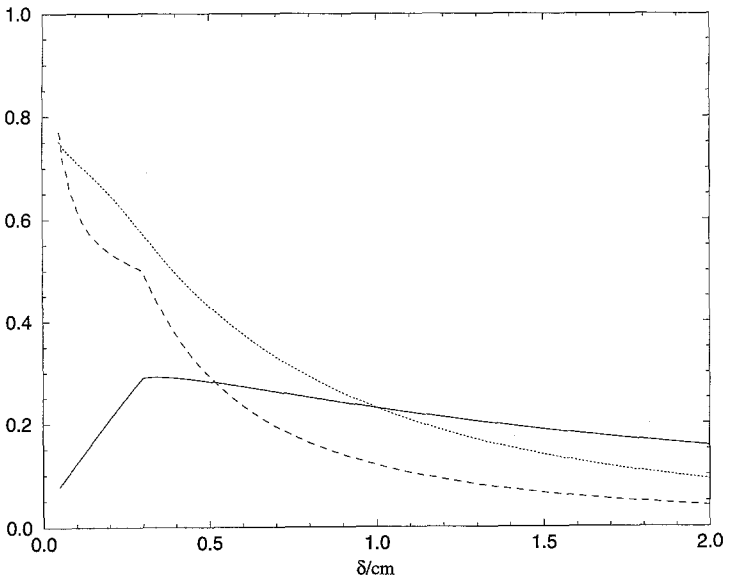

Fig. 11. Effect of varying interelectrode separation. Key: (——) i_{avg}/A cm^{-2}; (·····) f_{avg}; (— — —) total acetate conversion.

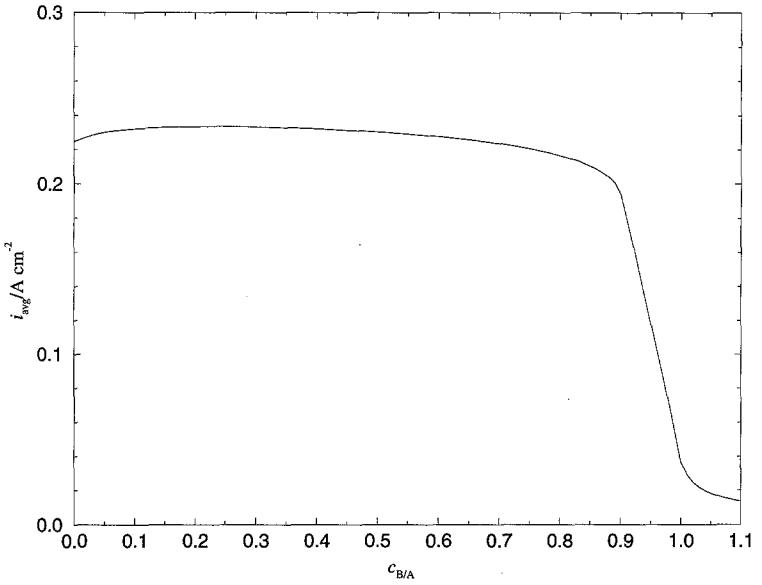

Fig. 12. Effect of varying base-to-acid ratio of the feed.

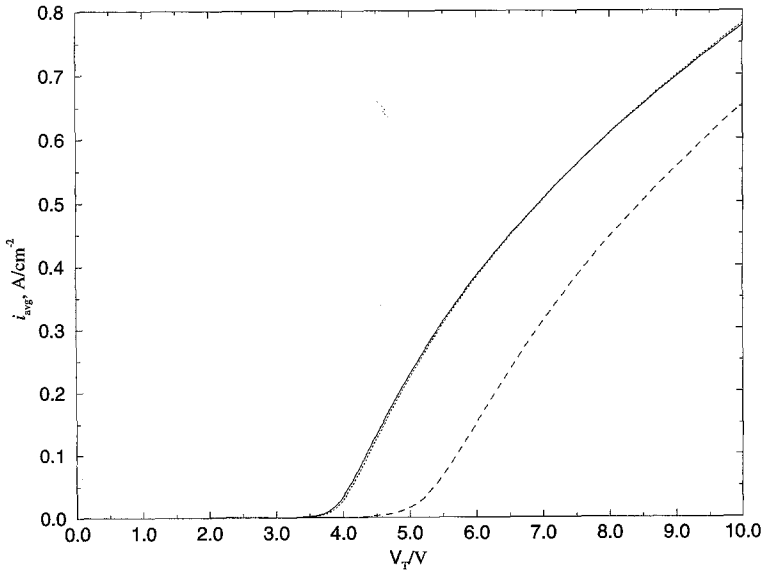

Fig. 13. Cell polarization curves at various base-to-acid ratios of the feed. Key: (·····) $c_{B/A} = 0$; (——) $c_{B/A} = 0.5$; (– – –) $c_{B/A} = 1.0$.

0.35 cm the current decreases because of the increased ohmic loss due to the longer ionic pathway. An optimal interelectrode separation for gas-evolving reactors has previously been reported by Tobias [16]. Nagy [17], and Nishiki *et al.* [18]. The total acetate conversion decreases monotonically with increasing electrode separation since the ratio of electrode area to flowrate decreases; however, the qualitative behaviour of the rate of change is different on either side of the optimum.

The effect of the base-to-acid ratio of the feed on the average current density is shown in Fig. 12. After an increase in current in the absence of base due to the increasing acetate concentration (Fig. 3), there is no significant change after the broad maximum near 0.23 until the ratio is approximately 0.85; thereafter, there is a rapid decrease in the current as the ratio approaches unity because of the decreased proton concentration (Fig. 3). Figure 12 was calculated assuming a constant value for the bubble-free solution resistivity. However, it is reasonable to anticipate that the bubble-free resistivity initially decreases with an increasing base-to-acid ratio as greater ionization occurs, reaches a minimum, and then increases due to increased solution viscosity. Such effects can be incorporated into a refinement of the present model, and we expect in doing so that the maximum current will become more pronounced.

Figure 13 illustrates the effect of cell potential on the average current density at three values of the base-to-acid ratio of the feed. Because of the assumed absence of mass-transfer resistance, the average current density continually increases with cell potential. The relationship between the two, however, is not linear at high cell voltage due to the nonlinear dependence of the solution resistance on the gas–void fraction. In addition, the reaction current distribution becomes more nonuniform as the cell voltage increases, and the majority of the reactor is inactive because of the gas evolved. At any given cell voltage, the average current density at $c_{B/A} = 1$ is the lowest of the three due to the diminished proton concentration. And, although not pronounced, there is a 'crossover' in Fig. 13 for the results for $c_{B/A} = 0$ and 0.5; that is, below ~7 V the current for $c_{B/A} = 0.5$ is greater than that for $c_{B/A} = 0$, but the trend is reversed at a higher voltage. The inlet current density for $c_{B/A} = 0.5$ is slightly higher than that for $c_{B/A} = 0$ for all cell potentials, as shown in Fig. 4; however, the average gas-void fraction for $c_{B/A} = 0.5$ is higher than that for $c_{B/A} = 0$. This causes the current density of $c_{B/A} = 0.5$ to decrease more quickly in the streamwise direction than that with $c_{B/A} = 0$ and thus a lower average current density for $c_{B/A} = 0.5$ for cell potentials higher than about 7 V.

For further refinement of the present model, several factors should be considered. These include the incorporation of mass-transfer resistance from the bulk solution to electrode surfaces and the dependence of the base-to-acid ratio on the bubble-free resistivity. Furthermore, to predict the current efficiency, side reactions, for example, Hofer–Moest reaction for alcohol formation, must be considered.

5. Summary

A model has been developed to study the Kolbe reaction of acetate in a parallel-plate reactor operating at a fixed cell potential. A parametric study demonstrated that the average current density is sensitive to cell geometry (interelectrode separation), operating conditions (inlet solution velocity and cell potential), and feed composition (base-to-acid ratio). The average current density increases with inlet solution velocity but approaches an asymptotic, secondary-current distribution limit which is equal to the reaction current density at the inlet. The average current density increases with cell potential but is not linear at high voltage because of the gas–void effect on solution resistance. The average current density has a maximum value with the interelectrode separation. There is also a broad maximum when the base-to-acid ratio is approximately 0.23; however, there is a large decrease in the average current density when the ratio approaches unity.

Acknowledgement

This work was made possible by financial support from the DuPont Company.

References

[1] A. V. Vijh and B. E. Conway, *Chem. Rev.* **67** (1967) 623.
[2] H. Vogt, *in* 'Comprehensive Treatise of Electrochemistry', Vol. 6, E. Yeager (edited by J. O'M. Bockris, B. E. Conway and S. Sarangapani) Plenum, New York (1983).
[3] P. J. Sides, *in* 'Modern Aspects of Electrochemistry', No. 18 (edited by R. E. White, J. O'M. Bockris, and B. E. Conway) Plenum, New York (1986).
[4] F. Beck, *Electrochim. Acta* **18** (1972) 359.
[5] M. Seko, A. Yomiyama and T. Isoya, *Hydrocarbon Processing*, No. 12 (1979) 117.
[6] Y. B. Vassiliev, E. P. Kosvman and G. N. Freidlin, *Electrochim. Acta* **27** (1982) 937.
[7] J. E. Funk and J. F. Thorpe, *J. Electrochem. Soc.* **116** (1969) 48.
[8] Yu. B. Vassiliev and V. A. Grinberg, *J. Electroanal. Chem.* **308** (1991) 1.
[9] W. E. Ryan, R. E. White and S. L. Kelly, *ibid.* **134** (1987) 2154.
[10] J. F. Yan, T. V. Nguyen, R. E. White and R. B. Griffin, *ibid.* **140** (1993) 733.
[11] R. E. Meredith and C. Tobias, *in* 'Advances in Electrochemistry and Electrochemical Engineering', Vol. 2 (edited by C. Tobias), Interscience Publishers, New York (1962).
[12] 'FORTRAN Subroutine for Mathematical Applications', IMSL, Math/Library, Houston, TX (1987).
[13] H. H. Uhlig and R. W. Revie, 'Corrosion and Corrosion Control', 3rd. edn., John Wiley & Sons, New York (1985).
[14] A. V. Vijh and B. E. Conway, *Z. Anal. Chem.* **224** (1967) 160.
[15] S. H. Maron and J. B. Lando, 'Fundamentals of Physical Chemistry', Macmillan, New York (1974).
[16] C. W. Tobias, *J. Electrochem. Soc.* **106** (1959) 833.
[17] Z. Nagy, *J. Appl. Electrochem.* **6** (1976) 171.
[18] Y. Nishiki, K. Aoki, K. Tokuda and H. Matsuda, *J. Appl. Electrochem.* **16** (1986) 615.